

PARTICLE ENGULFMENT AND PUSHING BY SOLIDIFYING INTERFACES - RECENT THEORETICAL AND EXPERIMENTAL DEVELOPMENTS

D.M. Stefanescu*¹, A.V. Catalina², F.R. Juretzko¹, S. Sen², P.A. Curreri³

¹ The University of Alabama, Tuscaloosa, AL 35487

² Universities Space Research Association, Huntsville, AL 35805

³ NASA Marshall Space Flight Center, Huntsville, AL 35812

Abstract

The objective of the work on Particle Engulfment and Pushing by Solidifying Interfaces (PEP) include 1) to obtain fundamental understanding of the physics of particle pushing and engulfment, 2) to develop mathematical models to describe the phenomenon, and 3) to perform critical experiments in the microgravity environment of space to provide benchmark data for model validation. Successful completion of this project will yield vital information relevant to a diverse area of terrestrial applications. With PEP being a long term research effort, this report will focus on advances in the theoretical treatment of the solid/liquid interface interaction with an approaching particle, experimental validation of some aspects of the developed models, and the experimental design aspects of future experiments to be performed on board the International Space Station.

Introduction

The study of particle behavior at solid/liquid interfaces (SLI's) is at the center of the *Particle Engulfment and Pushing* (PEP) research program. Interactions of particles with SLI's have been of interest since the 1960's, starting with geological observations, i.e., frost heaving. Ever since, this field of research has evolved as being significant to metal matrix composite materials, fabrication of superconductors, inclusion control in steels, and many other fields. The PEP research effort is geared to understand the fundamental physics of the interaction between particles and a planar SLI. Experimental work including 1-g and μ -g experiments accompany the development of analytical and numerical models and have already been presented elsewhere^{1,2,3}.

Real-time X-ray studies of SLI interaction with a second phase, i.e., gas pores and insoluble particles, are used to investigate the influence of the thermal and solutal field on the SLI morphology and the subsequent effect on the critical velocity of engulfment and will be presented here. The modeling efforts have grown from the initial steady-state analytical model to dynamic models, accounting for the initial acceleration of a particle at rest by an advancing SLI. To gain a more comprehensive understanding, numerical models were developed to account for the influence of the thermal and solutal field, on the critical velocity of engulfment. Some of these results will be presented in the theoretical part of this paper. Current efforts are geared towards the numerical calculation of the drag force and to couple the diffusive 2-D front tracking model with a fluid flow model to account for differences in the critical velocity of engulfment in 1-g and μ -g environments.

Keywords: particle pushing, interface tracking, interface morphology, μ -g experiments

*Corresponding author e-mail: doru@coe.eng.ua.edu

Theoretical

The theoretical problem is to accurately track the sharp and arbitrarily shaped SL interfaces. Finding an adequate solution to this problem is an important and necessary step, because it can open new possibilities to study the micro-scale phenomena occurring during the solidification. Morphological stability, coarsening processes and SL interface interaction with gaseous or non-metallic inclusions are only a few examples of phenomena that existing numerical solidification models cannot accurately describe. Amongst the various interface tracking techniques developed to date the *boundary-fitted coordinates*^{4,5,6} and the *phase-field*^{7,8,9} methods are the most notable. However, the boundary-fitted coordinates method experiences difficulties when dealing with highly distorted interfaces. It requires remeshing as the interface changes its shape. The phase-field method can use only a simple finite-difference technique, a fixed grid and does not require remeshing. However, it is computationally intensive and produces only diffuse interfaces. In addition, the several constants and parameters involved in the model are difficult to correlate to real physical systems. Because of the weaknesses of these methods, Udaykumar and Shyy^{10,11,12} have proposed a new technique based on a finite volume formulation. The moving SL interface is represented by a discrete set of markers that are positioned at the intersection of the interface with the grid lines. In this manner, after each iteration only the interface must be reconstructed. However, the requirement of redefinition of the control-volumes near the interface considerably increases the difficulty of model implementation and makes it susceptible to numerical errors. Our new approach uses the finite-difference formulation thus eliminating the need for control-volumes redefinition at the interface. It also includes the capability to track the interface during the solidification of alloys^{13,14}.

Directional solidification of pure aluminum in the vicinity of a spherical ZrO₂ particle of radius $R_p = 22.5 \mu\text{m}$ was chosen as a first case study. The imposed solidification velocity was $V = 2 \mu\text{m/s}$ under a thermal gradient in the liquid $G_L = 7 \text{ K/mm}$. The calculations were performed on a sample of length $L = 2 \text{ mm}$ and a width W which was varied, from case to case, from 1 mm to 0.4 mm in order to test its influence on the evolution of the SL interface shape. However, no noticeable effect was observed. At the beginning of the calculations (*i.e.*, $t = 0$) it was considered that at one end of the sample a slice of $\Delta z = 10 \mu\text{m}$ thickness was in solid state and that the SL interface was perfectly planar. The center of the particle was placed at $x = W/2$ and $z = \Delta z + h_c$, where h_c is the distance between the particle center and the planar SL interface (Fig. 1).

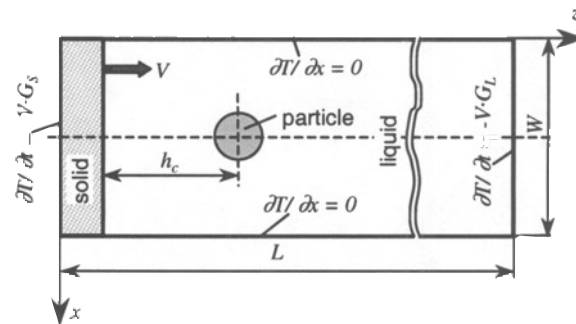


Fig. 1. The geometry and boundary conditions for the sample used in computations

Insulated boundary conditions were used on the x -direction while at the two ends of the sample constant cooling rates were considered. The cooling conditions were set such as to maintain the imposed solidification velocity, V , of the originally planar interface for the entire duration of the calculations. They were $\partial T/\partial x = -V \cdot G_L$ at the liquid end and $\partial T/\partial x = -V \cdot G_s$ at the solid end, where G_s is the temperature gradient in the solid phase.

The available analytical solution for a problem of this type¹⁵ predicts that when the thermal conductivity of the particle, k_p , is smaller than that of the liquid, k_L , the SL interface will become convex toward the particle, forming a bump as it approaches the particle. Indeed, our numerical calculations show this behavior as can clearly be observed in Fig. 2 and Fig. 3.

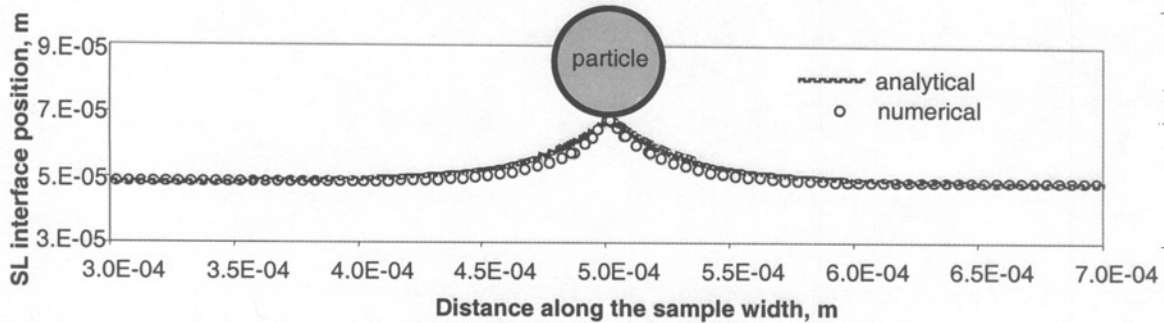


Fig. 2. SL interface shape: comparison of analytical and numerical solutions (pure Al, ZrO_2 particle $R_p = 22.5 \mu\text{m}$, $V = 2 \mu\text{m/s}$, with no Gibbs-Thomson effect)

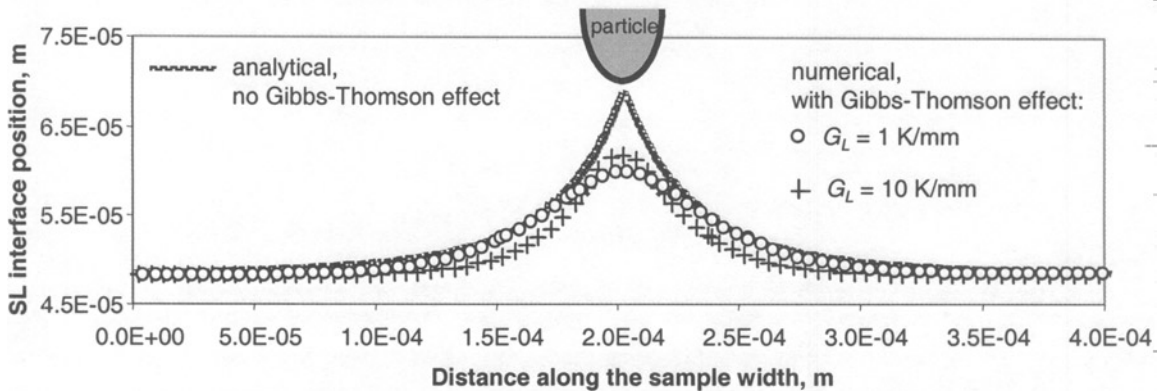


Fig. 3. Influence of the Gibbs-Thomson effect and the temperature gradient, G_L , on the shape of the SL interface (pure Al, ZrO_2 particle $R_p = 22.5 \mu\text{m}$, $V = 2 \mu\text{m/s}$). For a better view of the interface deformation non-equal scales were used on the vertical and horizontal directions, leading to the non-circular appearance of the sphere.

Fig. 2 shows a comparison between the numerical and the analytical solutions when neglecting the Gibbs-Thomson effect (*i.e.*, $\Gamma = 0$). The agreement is good, thus proving the capability of the proposed interface tracking model. In all our numerical simulations, the interface perturbation is somewhat sharper than that predicted by the analytical solution. This is mainly because of the insulated boundary conditions used at a finite distance from the particle (see Fig. 1) as compared to the analytical solution which implies that $\partial T/\partial x = 0$ occurs at $x \rightarrow \infty$.

Fig. 3 shows the shape of the SL interface when accounting for the Gibbs-Thomson effect. It can be observed that, as expected, the amplitude of the interface perturbation becomes considerably smaller as compared to the case when $\Gamma = 0$. The influence of the temperature gradient, G_L , is also shown on this figure. As G_L increases, the perturbation becomes sharper and its amplitude also increases. This implies that the perturbation develops faster when increasing G_L .

The Influence of Solute

The first test-problem that we consider in this case is the solute redistribution during the initial transient of plane front directional solidification of a binary alloy. An analytical solution to this problem¹⁷ shows that the concentration profile, $C_s(z)$, in the solidified sample can be expressed as:

$$C_s(z) = \frac{C_o}{2} \left\{ 1 + \operatorname{erf} \left[\frac{\sqrt{(V/D_L)} \cdot z}{2} \right] + (2k-1) \cdot e^{k(k-1)(V/D_L)z} \cdot \operatorname{erfc} \left[\frac{2k-1}{2} \sqrt{(V/D_L)} \cdot z \right] \right\}$$

Eq. 1

where C_o is the initial concentration in the liquid sample, z is the distance measured from the beginning of the sample along the solidification direction, and erf and erfc are the error and complementary error functions, respectively.

The results shown in Fig. 4 are for Sn-0.5 at% Bi alloy at $V = 4.9 \mu\text{m/s}$ and a thermal gradient in the liquid $G_L = 17.3 \text{ K/mm}$. The numerical calculations were performed for a sample of length $L = 10 \text{ mm}$ and width $W = 20 \mu\text{m}$ using a grid size of $4 \mu\text{m}$. In order to maintain the imposed solidification velocity and temperature gradients for the entire duration of the calculations the following boundary conditions for the temperature at the two ends of the sample have been used:

• at the liquid end

$$\text{Eq. 2} \quad \frac{\partial T}{\partial t} = - \left(V \cdot G_L + m_L \frac{\partial C_L^l}{\partial t} \right)$$

• at the solid end

$$\text{Eq. 3} \quad \frac{\partial T}{\partial t} = - \left(V \cdot G_S + m_L \frac{\partial C_L^l}{\partial t} \right)$$

where $\partial C_L^l / \partial t$ represents the time change of the liquid concentration at the SL interface. Insulated boundary conditions for both temperature and concentration were used on the x -direction as shown in Fig. 1.

A good agreement between the analytical solution and the numerical results can be observed in Fig. 4. In addition, the experimental measurements of Favier *et al*¹⁶ performed on a sample solidified in micro-gravity conditions are also in good agreement with our numerical results.

With the numerical model validated against analytical solutions and experimental results for the solidification of binary alloys we can proceed to study the evolution of the SL interface shape when a foreign particle is added to the melt in front of the interface. We chose Al-2 wt% Cu for the alloy and ZrO_2 for the particle. A steady-state distribution for the solute and linear distribution for the temperature was considered as initial conditions. The boundary conditions for temperature are presented in Fig. 1. Insulated boundary conditions on the x -direction as well as on the surface of the particle were added for the solute.

While for the solidification of pure substances our numerical calculations as well as the analytical solution¹⁹ show that the solidification velocity has a negligible effect on the evolution of the SL interface near a foreign particle, this conclusion cannot be extended to solidification of alloys. The influence of the solidification velocity is shown in Fig. 5. The solute trapping in the particle/interface gap becomes more significant with the increase of the solidification velocity and therefore the depth of the concavity formed

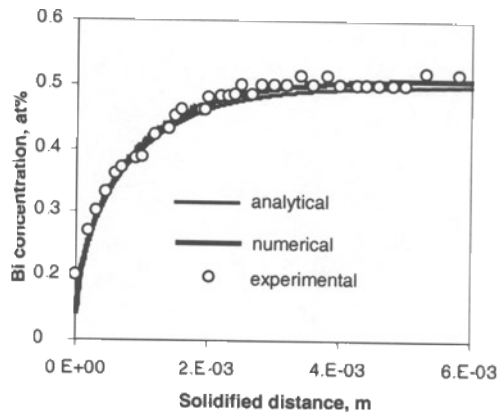


Fig. 4. Numerical predictions vs. analytical solution¹⁷ and experimental measurements¹⁸ for Bi segregation during the initial transient plane front solidification ($V = 4.9 \mu\text{m/s}$) of Sn-0.5 at% Bi on the SL interface beneath the particle will be higher at higher solidification velocity. On the other hand, when measured with respect to the flat region of the interface, the amplitude of the two humps that form on both sides of the vertical centerline is smaller at higher velocities. Thus, the solute effect becomes predominant over the thermal effect (quantified through the ratio k_p/k_L) when increasing the solidification velocity. Note that for the velocity $V = 2 \mu\text{m/s}$, used to generate Fig. 5, the stability theory²⁰ predicts that the SL interface is inherently unstable and perturbations other than induced by the presence of the particle should also appear on the interface. This is true and we have demonstrated²¹ that the present model has the capability to describe the development of such perturbations. For the case presented in Fig. 5, however, where the sample width, W , was considered of only 0.4 mm the perturbations induced by the presence of the particle override the perturbations that would have been induced by the constitutional undercooling effect alone.

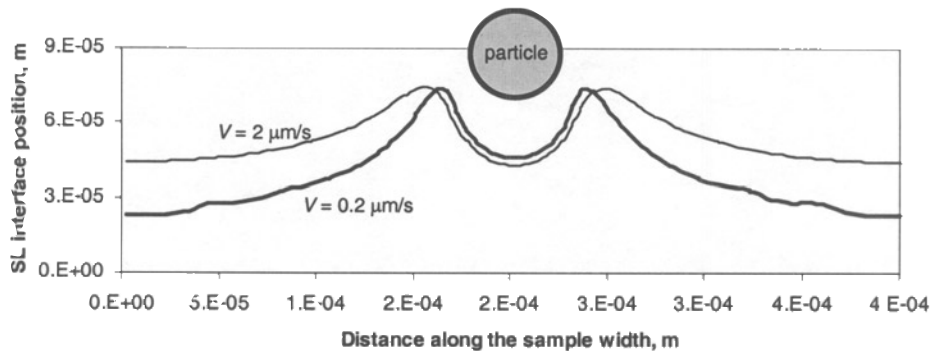


Fig. 5. Influence of the solidification velocity on the shape of the SL interface when approaching a foreign particle (Al-2 wt% Cu, ZrO_2 particle, $R_p = 22.5 \mu\text{m}$, $G_L = 7 \text{K/mm}$)

Experimental

Ground based work

To validate the model described in the theoretical part, the dynamics of the interaction between a gas pore and a solidification front in metal alloys was observed using a state of the art X-ray Transmission Microscope. The experiments included observation of the distortion of the SL interface near a pore, real-time measurements of the growth rate and the change in shape of the porosity during interaction with an advancing SL interface in pure Al and Al-0.25 wt% Au alloy. In addition, porosity induced solute

segregation patterns surrounding a pore were also quantified with the model system Al-0.25 wt% Au alloy. Fig. 6 shows a post-solidification radiograph of a pore after engulfment by a planar SL interface. The pore has an ellipsoidal shape with a size of about 800 μm along the major axis and 660 μm along the minor axis. The growth velocity was 5 $\mu\text{m}/\text{s}$ and the temperature gradient 4.7 K/mm. The purpose of this experiment was to investigate the effect of the pore on the solutal segregation pattern. The radiograph shows that there is a strong segregation of Au around the pore just prior to engulfment. The SEM micrograph (Fig. 6b) in the inset shows that the microstructure in this area consists of eutectic colonies. The eutectic structure inside one such colony is shown in Fig. 6c. The thickness of this eutectic ‘band’ varies between 70–80 μm . The centerline microprobe scan indicates that the Au composition in this region is approximately 8.0 wt%. This is in agreement with the equilibrium phase diagram for the Al-Au system, which shows a eutectic transformation at 7.46 wt. % Au. Subsequent to engulfment of the pore, a comet tail shaped segregation pattern is clearly evident on the left of the pore (Fig. 6a).

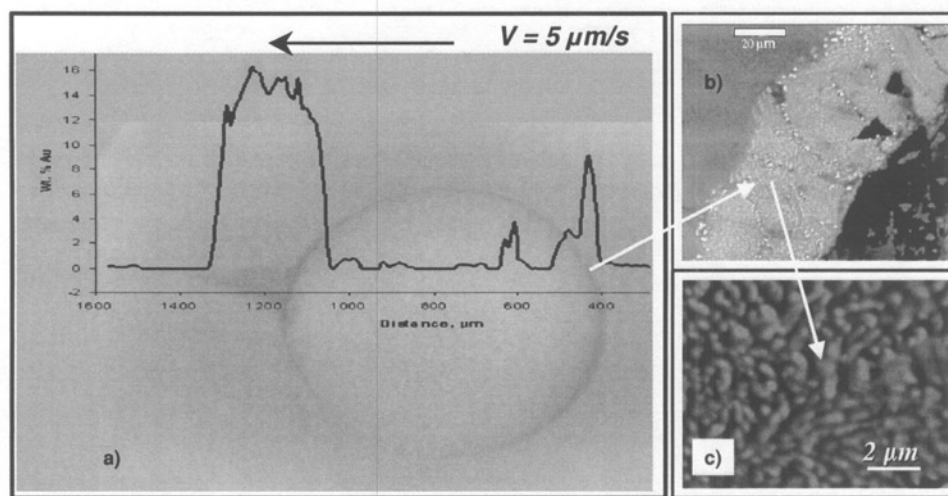


Fig. 6. Post-solidification radiograph showing segregation of Au around the porosity. Superimposed is a centerline microprobe scan.

In its current stage, the previously described model does not have the capability to account for changes of pore size and shape during the interaction with the SL interface. Therefore, only spherical pores of constant radius have been used in the present numerical modeling. Fig. 7 shows the calculated shape of the SL interface in various stages of a H_2 pore engulfment by the solid phase. The occurrence of a trough on the SL interface after engulfment is also observed. This is typical when the thermal conductivity of the particle (H_2 pore in this particular case) is smaller than that of the metallic matrix.

For the solidification of the Al-0.25 wt% Au alloy our calculations also predict that at a distance from the pore similar to that experimentally observed, the Au concentration raises to the eutectic value, as shown in Fig. 8. Fig. 9 shows a three-dimensional view of the Au concentration profile around the pore when the concentration in the pore/SL interface gap reaches the eutectic value.

At this stage, the concentration behind the pore, in the vicinity of the centerline of the sample, is smaller than in the regions away from the centerline. This is expected because the solute cannot diffuse through the pore. Currently, a model for eutectic solidification is not yet implemented in our numerical program and therefore the computation was stopped when Au concentration in the liquid pore/SL interface gap

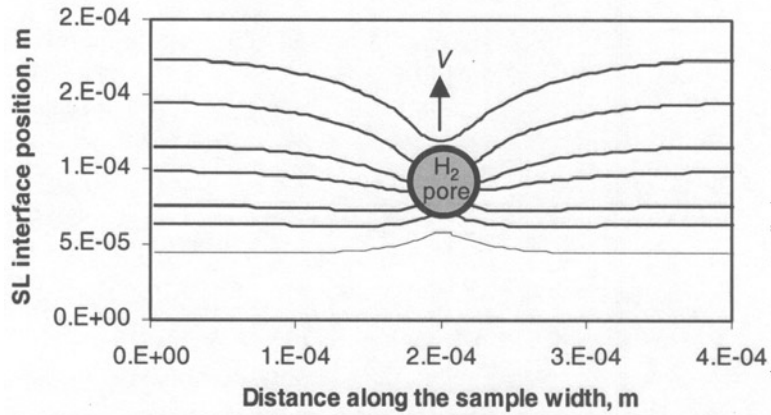


Fig. 7. Numerically calculated shape of the SL interface in various stages of engulfing a H_2 pore of fixed size (pure Al, $R_{pore} = 22.5 \mu\text{m}$, $V = 4 \mu\text{m/s}$, $G_L = 4.7 \text{ K/mm}$)

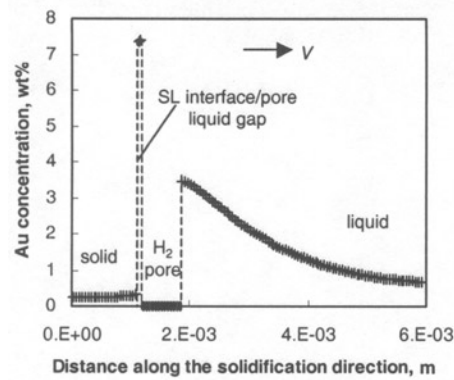


Fig. 8. Numerically calculated Au distribution profile along the sample centerline showing solute trapping in the SL interface/pore gap (Al-0.25 wt% Au, $V = 5 \mu\text{m/s}$, $G_L = 4.7 \text{ K/mm}$)

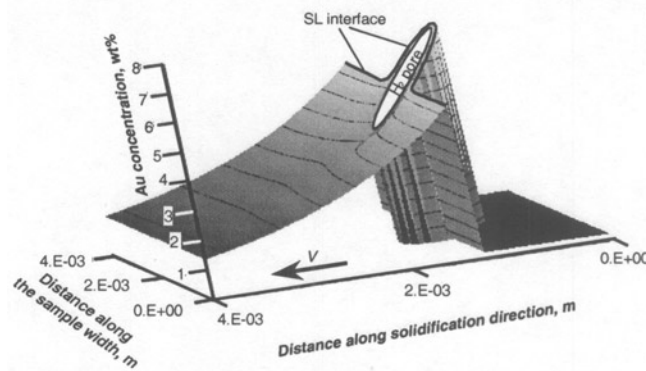


Fig. 9. Calculated Au concentration profile around a H_2 pore when the concentration in the pore/SL interface gap reaches the eutectic value (Al-0.25 wt% Au, $V = 5 \mu\text{m/s}$, $G_L = 4.7 \text{ K/mm}$, $R_{pore} = 330 \mu\text{m}$) reached the eutectic value. This precluded a quantitative prediction of the second region of strong Au segregation developed in front of the pore after its complete engulfment.

Preparation for flight experiment

To obtain the necessary benchmark data for model validation, it is planned to have two sets of experiments on board the ISS. The first set consists of eight directional solidified samples in the quench module 592

insert (QMI) facility. This facility is a NASA-build module situated in the MSRR, Fig. 10. The sample-ampoule-cartridge-assembly (SACA) will contain the sample and the necessary instrumentation. It is planned to have two different designs available to perform directional solidification experiments with and without quench. The first set of experiments is designed to map the behavior of inert particles of different radii for pure metals and for solid-solution alloys. The second set will use the quenching capabilities of the QMI and is planned to capture the pushed particles at the solid/liquid interface of both pure matrices and alloy matrices, including the changes of the solutal field for the latter.

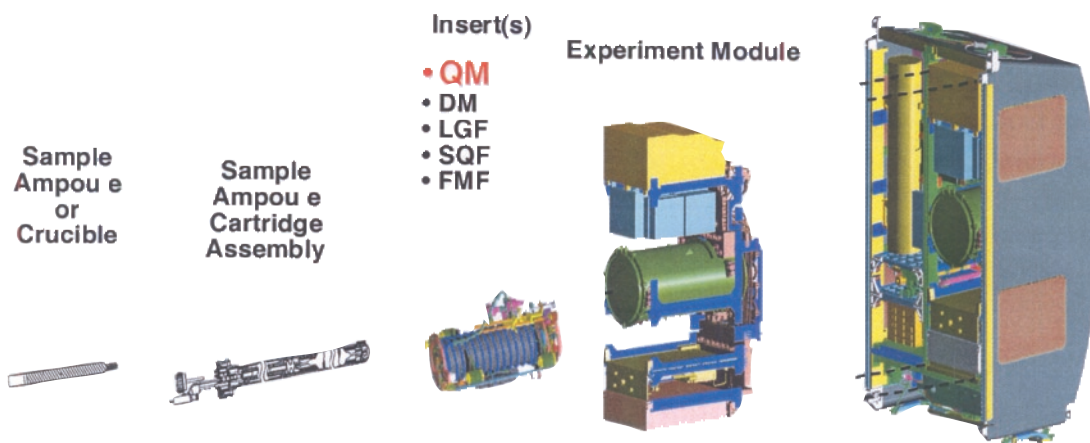


Fig. 10. Exploded view of the sample location within the Material Science Research Rack.

The material selection for the particles is zirconia of radii varying from 50 to 250 μm . The selection for the matrix materials is pure aluminum and zinc. To study the influence of the solutal field on the pushing-engulfment transition, solid-solution aluminum alloys were selected. An overview of the experiments planned for the first stage is given in Table 1.

The early flight opportunity provided by the LMS mission in 1996 enabled the testing of several experiment design options. Among these were the design of the ampoule, containing the liquid metallic sample and the subsequent task of free surface management. During the LMS mission, two designs were explored, one featuring a spring and piston design, while the other used an expansion void. The spring and piston design worked flawless in the $\mu\text{-g}$ environment and yielded a sound sample²². It is currently planned to use this design for the management of the free surface inside the ampoule. The drawback of this design is the requirement of tight tolerances between the ceramic piston and the ceramic ampoule to prevent any passage of the liquid metal and subsequent contact of the metal with the graphite spring. At the operating temperature, this would cause a reaction of the graphite with the aluminum metal and lead to the immobilization of the piston. Plans were developed for an alternative ampoule design where the spring is located in the cold zone. This requires for the ampoule to move within the cartridge and to have a perfectly sealed piston at the hot end, Fig. 11. This design, if successfully implemented, might provide an interesting solution to the challenges set forth by the spring and piston design.

Table 1. Matrix of the first set of PEP experiments to be processed without quench.

No.	Matrix	Particle		Solidification velocity, $\mu\text{m/s}$	Processed length, mm	Processing time, hrs
		type	radius, μm			
1	Al	ZrO ₂	50, 100, 250	0.3, 0.6, 1.2, 2.4, 4.8	125	44.82
2	Al	ZrO ₂	50, 100, 250	4.8, 10, 15, 20, 30	125	3.16
3	Zn	ZrO ₂	50, 100, 250	0.3, 0.6, 1.2, 2.4, 4.8	125	44.82
4	Zn	ZrO ₂	50, 100, 250	4.8, 10, 15, 20, 30	125	3.16
5	Al-Cu or Mg	ZrO ₂	50, 100, 250	0.1, 0.3, 0.6, 1.0, 1.5	125	99.5
6	Al-Cu or Mg	ZrO ₂	50, 100, 250	1.5, 2.0, 2.5, 3.2	135	17.32
7	Al-Ni eutect.	ZrO ₂	50, 100, 250	0.1, 0.3, 0.6, 1.0, 1.5	125	99.5
8	Al-Ni eutect.	ZrO ₂	50, 100, 250	1.5, 2.0, 2.5, 3.2	135	17.32

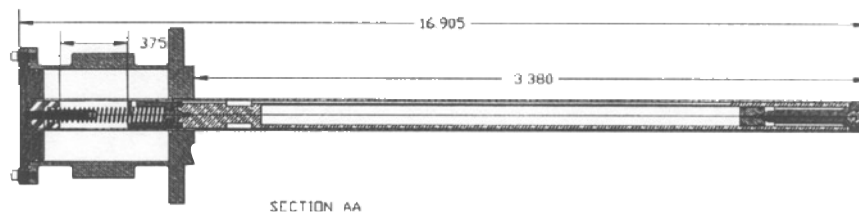


Fig. 11. Technical drawing of the alternative SACA concept with the spring located in the cold zone²³.

Other experimental design issues resolved by the experiments on LMS were the decision of the proper velocity profiles. It was found that a stepwise increase yielded better interface velocity control than a stepwise decrease. This is of importance when only a limited length of the sample can be used.

Based on the limitation of the experiment module (EM) and subsequently the QMI dimensions, the sample dimensions and further design criteria are given in Table 2. The quenching capabilities are based on a unique phase change device, which will be part of the SACA itself. This device features radially placed low melting point alloy blocks, which can be released onto the cartridge.

Table 2. Design criteria for the PEP experiment on board the ISS

Sample diameter	8 to 10 mm
Processing length	max. 200 mm, 150 mm with quench
Maximum processing temperature	900°C
Temperature gradient	<i>pure metals</i> 70°C/cm <i>alloys</i> 100°C/cm
Translation range	0.1 to 30 $\mu\text{m/s}$
Atmosphere	inert gas
Quench rate	ability to solidify within 2s with no melt-back of a 5mm axial section
Microgravity environment	10 ⁻⁴ g _o or less
Sample instrumentation	11 thermocouples

Contribution of the PEP project to Education and the Scientific Community

After its inception on the early 1990's, NASA has provided the PEP research effort with two shuttle experiments and the possibility of using the QMI on board the ISS. In reflection of NASA's agenda, the projects are expected to serve the furthering of scientific knowledge and the continuous education of future scientist. In light of these objectives, the PEP team has published 38 papers in journals and conference proceedings, the overwhelming majority of which are peer reviewed. An indicator of the scientific contribution of this research effort is the number of independent citations in refereed scientific journals, which, from 1990 to June 2001 were counted to be 247, Fig. 12. In addition, under the funding of this research effort nine (9) masters degrees were awarded, as were three (3) Ph.D. degrees.

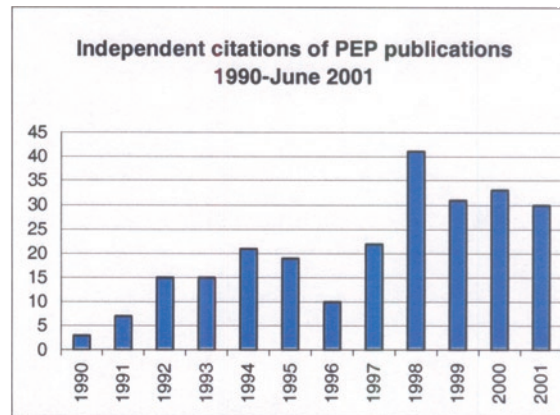


Fig. 12. Independent citations in refereed publications till June 2001

Acknowledgements

The help and dedication of the crews of STS-78 and STS-87 are gratefully acknowledged. The technical support of Tec-Masters Inc. has been and is acknowledged, as is the help of innumerable NASA personnel and students at The University of Alabama over the past years.

Support by the NASA Office of Biological and Physical Sciences under NAS8-00207.

References

1. F.R. Juretzko, B.K. Dhindaw, D.M. Stefanescu, S. Sen and P.A. Curreri, *Metall. Mat. Trans.*, vol. 29A, June 1998, pp. 1691-1696
2. D.M. Stefanescu, F.R. Juretzko, B.K. Dhindaw, A.V. Catalina, S. Sen and P.A. Curreri, *Metall. Mat. Trans.*, vol. 29A, June 1998, pp. 1697-1706
3. S. Sen, F.R. Juretzko, D.M. Stefanescu, P.A. Curreri *J. Crystal Growth*, vol. 204, June 1999, pp.238-242
4. L.N. Brush and R.F. Sekerka: *J. Crystal Growth*, 1989, vol. 96, pp. 419-41
5. M. Lacroix: *Num. Heat Transf. B*, 1989, vol. 15, pp. 191-210
6. C.H. Kuo and W.C. Schreiber: *HTD*, 1994, vol. 275, pp.57-64
7. S.L. Wang, R.F. Sekerka, A.A. Weeler, B.T. Murray, S.R. Coriel, R.J. Braun, and G.B McFadden: *Physica D*, 1993, vol. 69, pp.189-200
8. J.A. Warren and W.J. Boettinger: *Acta metal. mater.*, 1995, vol. 43, no. 2, pp. 689-703
9. W.J. Boettinger and J.A. Warren: *Metall. Mat. Trans. A*, 1996, vol. 27A, pp. 657-69
10. W. Shyy, H.S. Udaykumar, M. M. Rao, and R.W. Smith: *Computational Fluid Dynamics with Moving Boundaries*, Taylor & Francis, Washington, DC, 1996
11. H.S. Udaykumar and W. Shyy: *Numerical Heat Transfer B*, 1995, vol. 27, pp. 127-53

12. H.S. Udaykumar and W. Shyy: *Int. J. Heat Mass Transfer*, 1995, vol. 38, no. 11, pp. 2057-73
13. A.V.Catalina, D.M.Stefanescu, S.Sen, W.K.Kaukler, submitted to *Metall. Mat. Trans. A*
14. A.V. Catalina and D.M. Stefanescu, in *Proceedings of the 4th Pacific Rim International Conference on Modeling of Casting & Solidification Processes*, C.P. Hong, J.K. Choi and D.H. Kim editors, CAMP, Seoul, Korea (2000) 3-12
15. A.V. Catalina, S. Mukherjee, and D.M. Stefanescu: *Metall. Mat. Trans. A*, 2000, vol. 31A, pp.2559-68
16. J.J. Favier, P. Lehmann, J.P. Garandet, B. Drevet, and F. Herbillon: *Acta mater.*, 1996, vol. 44, pp. 4899-907
17. V.G. Smith, W.A. Tiller, and J.W. Rutter: *Can. J. Phys.*, 1955, vol. 33, pp.723-45
18. J.J. Favier, P. Lehmann, J.P. Garandet, B. Drevet, and F. Herbillon: *Acta mater.*, 1996, vol. 44, pp. 4899-907
19. A.V. Catalina, S. Mukherjee, and D.M. Stefanescu: *Metall. Mat. Trans. A*, 2000, vol. 31A, pp.2559-68
20. W.W. Mullins and R.F. Sekerka: *J. Appl. Phys.*, 1964, vol. 35, no. 2, pp. 444-51
21. A.V. Catalina, S. Sen, D.M. Stefanescu, and P.A. Curreri: *Modeling of Casting, Welding and Advanced Solidification Processes IX*, P.R. Sahm, N. Hansen, and J.G. Conley eds., Aachen, Germany, 2000, pp. 445-52
22. D.M. Stefanescu, B.K. Dhindaw, F.R. Juretzko, P.A. Curreri and S. Sen, in *Life and Microgravity Spacelab (LMS) Final Report*, J.P. Downey compiler, Marshall Space Flight Center, Alabama (1998), pp.78-87
23. Barry Battista, Tec-Masters Inc. private communications, The University of Alabama, 2001